NANO LETTERS

pubs.acs.org/NanoLett Letter

Stretchable Nanolayered Thermoelectric Energy Harvester on Complex and Dynamic Surfaces

Yang Yang,[@] Hongjie Hu,[@] Zeyu Chen,[@] Ziyu Wang,* Laiming Jiang, Gengxi Lu, Xiangjia Li, Ruimin Chen, Jie Jin, Haochen Kang, Hengxi Chen, Shuang Lin, Siqi Xiao, Hanyu Zhao, Rui Xiong, Jing Shi, Qifa Zhou, Sheng Xu,* and Yong Chen*

Cite This: *Nano Lett.* 2020, 20, 4445−4453 Read Online

ACCESS | Metrics & More | Article Recommendations | Supporting Information

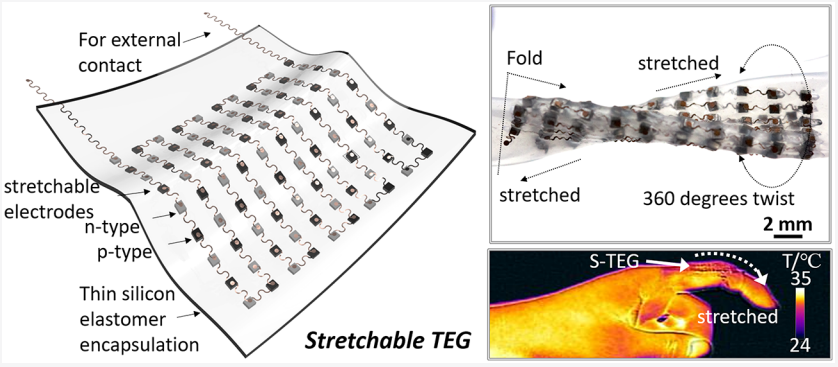

ABSTRACT: Thermoelectric generators (TEGs) provide a unique solution for energy harvesting from waste heat, presenting a potential solution for green energy. However, traditional rigid and flexible TEGs cannot work on complex and dynamic surfaces. Here, we report a stretchable TEG (S-TEG) (over 50% stretchability of the entire device) that is geometrically suitable for various complex and dynamic surfaces of heat sources. The S-TEG consists of hot-pressed nanolayered p-(Sb_2Te_3) and n-(Bi_2Te_3)-type thermoelectric couple arrays and exploits the wavy serpentine interconnects to integrate all units. The internal resistance of a 10 × 10 array is 22 ohm, and the output power is ~0.15 mW/cm^2 at ΔT = 19 K on both developable and nondevelopable surfaces, which are much improved compared with those of existing S-TEGs. The energy harvesting of S-TEG from the dynamic surfaces of the human skin offers a potential energy solution for the wearable devices for health monitoring.

KEYWORDS: *Stretchable thermoelectric generator, Nanolayered structure, Complex and dynamic surfaces, Green energy, Health monitoring*

Renewable energy sources such as geothermal power attract much attention as a sustainable electricity supply owing to the current increase of energy consumption and lack of fossil fuels in the world.[1−5] A major part of the heat from industrial processes and the human body is wasted.[6−8] A thermoelectric generator (TEG) can convert waste heat into usable electricity, which in turn helps improve energy efficiency through waste heat recovery.[9−11] Thermal energy harvesting may provide a fundamental energy solution for bioimplantable and wearable devices with small power requirements.[12−15]

The most widely used thermoelectric (TE) materials are metal oxides and heavily doped metallic alloys.[16,17] The traditional methods of fabricating TEG are zone melting and hot pressing, both of which generate a moderately high figure of merit (ZT) value.[1,2,18,19] However, both the energy conversion efficiency and the output power are highly related to the heat transfer between the heat source and the TEG, especially on complex and dynamic surfaces. The rigid and bulky TE materials by the traditional methods show ineffective heat transfer due to the nonconformal interfacial contact with the complex and dynamic surfaces.[20,21] Thus, the widespread application of TEG has been hindered by the challenges of close integration with complex and dynamic heat surfaces. To address this problem, many new types of TEGs have been developed, e.g., the shape-conformal[22−24] and flexible TEGs[25] can accommodate static developable surfaces. However, they are inapplicable for nondevelopable and dynamic surfaces.[26] Furthermore, for shape-conformal TEGs (by 3D printing and painting) and flexible TEGs, the electrical instability may cause

Received: March 19, 2020
Revised: April 27, 2020
Published: May 5, 2020

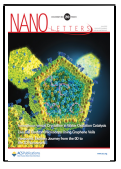

https://dx.doi.org/10.1021/acs.nanolett.0c01225
Nano Lett. 2020, 20, 4445−4453

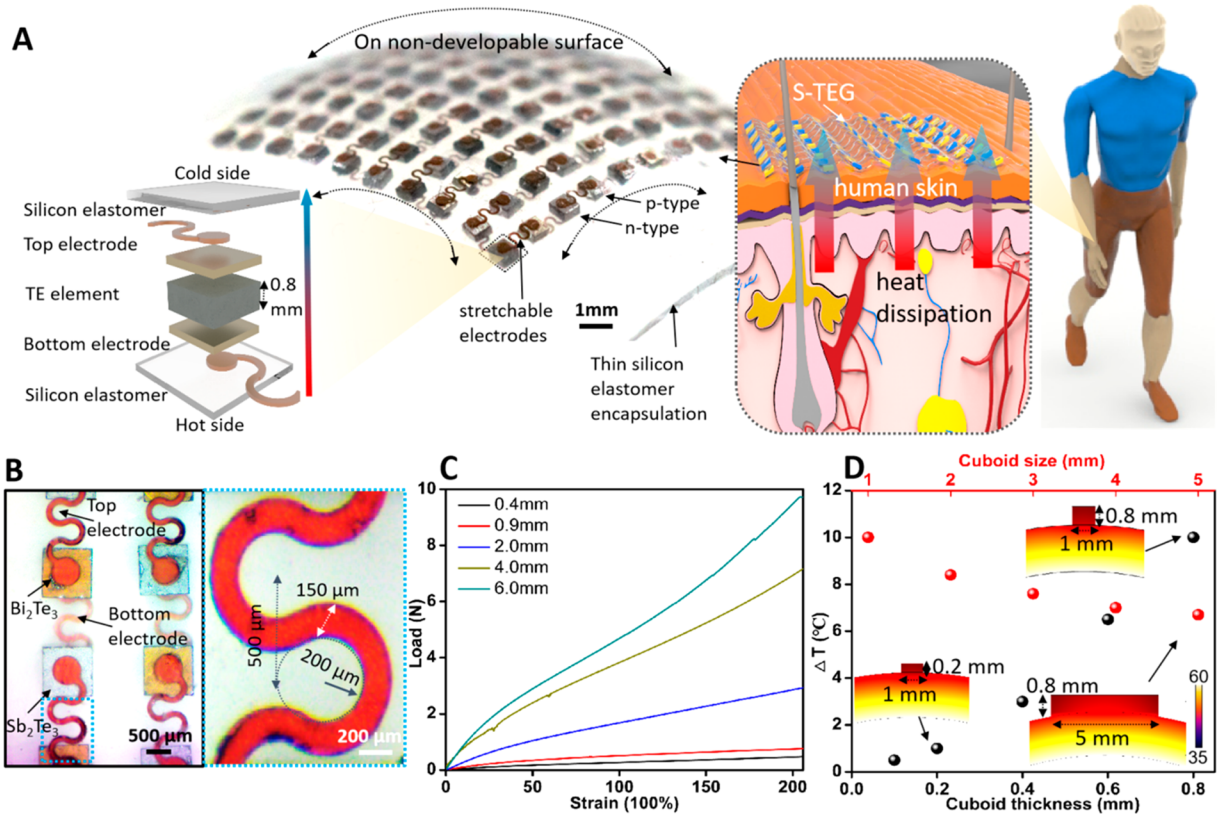

Figure 1. Design and application of the stretchable TEG (S-TEG). (A) The schematic diagram shows the energy harvesting of S-TEG from the waste heat of human skin; in the diagram, an optical image and an exploded schematic of the device show the 10 × 10 array p-n couples of TE materials and the components of one unit, respectively. (B) Optical images showing the layout of the S-TEG (left) and the design details of the serpentine electrode (right). (C) Load−strain curves for the Ecoflex with different thicknesses (all of the samples with the sizes of 25 mm × 25 mm). (D) Simulation of temperature differences (ΔT) of the top and bottom surfaces of the cuboids with different sizes and thicknesses (length in the range of 1−5 mm, thickness from 0.1 mm to 0.8 mm) attached on a convex surface.

critical problems during movement.[25,27,28] In comparison, stretchable TEGs can work on a dynamic surface, but the doped silicon or deposition of TE materials on paper/polymer-based substrates cause high internal resistance that leads to low output power density.[29−31] Currently, TEGs with a suitable structure that can geometrically match complex and dynamic heat surfaces remain to be a challenge.[20]

Here, we report a stretchable TEG (S-TEG) that is geometrically suitable for various complex and dynamic surfaces. These active elements of hot-pressed p-type (Sb_2Te_3) and n-type (Bi_2Te_3) cuboids were interconnected by the stretchable serpentine interconnection and embedded in the Ecoflex elastomer. The S-TEG keeps superior mechanical properties (with over 50% biaxial stretchability) and perfectly conforms to both developable and nondevelopable surfaces. The output power is much improved compared with other stretchable TEGs by minimizing the contact resistance between the cuboids and the electrodes (Table S1). The heat transfer from complex surfaces of heat sources to our S-TEG was simulated and compared with traditional planar TEGs. The performance of the developed S-TEG on complex surfaces and dynamic surfaces of the human body was studied.

Figure 1A shows a schematic diagram of the energy harvesting from the waste heat of human skin and the 10 × 10 TE couple array on a silicon matrix of 25 mm × 25 mm. The fabricated S-TEG was made of p-n legs connected thermally in parallel and electrically in series. The p-n cuboids were assembled with the "island-bridge" layout electrodes, embedded in the compliant and ultrastretchable silicone elastomer (Ecoflex) (Figure 1B).[32,33] The TE powders were hot-pressed into discs and diced into small cuboids (1 mm × 1 mm × 0.8 mm). Ecoflex with Young's modulus (~70 kPa) similar to that of human skin and super stretchability (~900%) was used to encapsulate the entire device. The 15 μm thickness of the substrate and superstrate provide mechanical support for the device. The Ecoflex with a thickness of 0.9 mm is much easier to be stretched to 200% strain (0.7 N) than that with 6 mm thickness (10 N for 200% strain) (Figure 1C). Besides, the dimensions of the cuboids were optimized by using Comsol Multiphysics to study the temperature difference of the top and bottom surfaces when attaching the TE cuboids to the convex surface (Figure 1D). To balance the thermoelectric performance and the stretchability of the device, the size of the cuboids was optimized to be 1 mm × 1 mm × 0.8 mm to exhibit both high ΔT and large stretchability. Stretchable electrodes were fabricated by laser ablation (Figure S1). Details of the S-TEG fabrication are illustrated in the Methods and Figure S3. The relatively flexible fabrication of the TE arrays on a stretchable substrate demonstrates the advantage of the design for large scale S-TEG. The mechanical robustness of the as-fabricated device is demonstrated in Figure S2 in which the device naturally bends on the developable (cylindrical) and nondevelopable surfaces (Figure 1A). It also can be folded, stretched, and twisted without breaking, showing its high endurance to the skin deformation.

https://dx.doi.org/10.1021/acs.nanolett.0c01225
Nano Lett. 2020, 20, 4445−4453

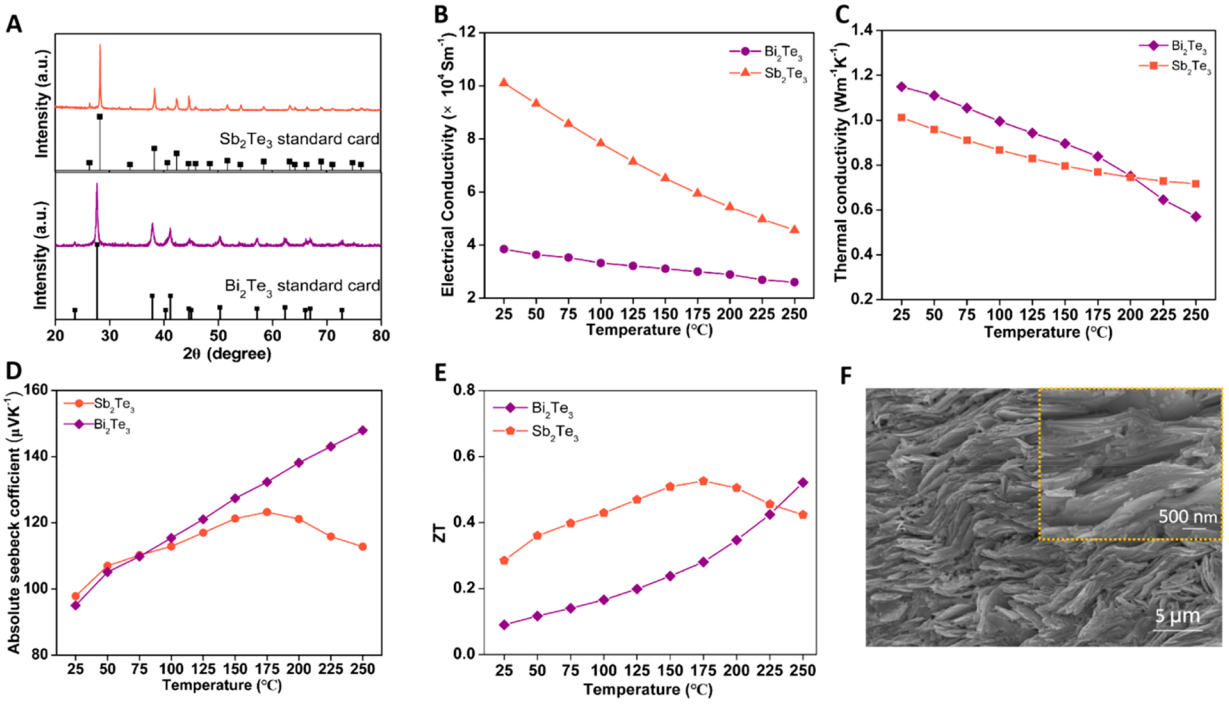

Figure 2. Thermoelectric characterizations. (A) Comparison of XRD patterns of Bi_2Te_3 and Sb_2Te_3 with the standard card; (B) electrical conductivity and (C) thermal conductivity of TE cuboids; (D) absolute Seebeck coefficient and (E) ZT values of Bi_2Te_3 and Sb_2Te_3 (with PEDOT:poly(styrenesulfonate) PSS); and (F) SEM images of hot-pressed Sb_2Te_3, showing the layered structure of Sb_2Te_3 after hot pressing.

The X-ray diffraction (XRD) patterns of the TE cuboids show characteristic peaks that correspond to Bi_2Te_3 and Sb_2Te_3, demonstrating the pure crystalline phases after hot pressing (Figure 2A). The electrical conductivities of the p-type and n-type cuboids at room temperature (RT) are 1.02×10^5 S m^{-1} and 3.98×10^4 S m^{-1}, respectively. The electrical conductivity is in the range of 5×10^4 to 1.02×10^5 S m^{-1} (p-type) and 2.7×10^4 to 3.98×10^4 S m^{-1} (n-type), respectively, and decrease with increasing temperature (Figure 2B). The thermal conductivity is in the range of 0.73−1.01 W m^{-1} K^{-1} (p-type) and 0.59−1.15 W m^{-1} K^{-1} (n-type), respectively, and decrease with increasing temperature (Figure 2C). The reduced thermal conductivity of Sb_2Te_3 (with PEDOT:poly(styrenesulfonate) PSS) is attributed to the scattering of phonons between the mesoscale boundaries between the two phases. In addition, the relatively high carrier concentrations lead to a weak bipolar contribution and a small negative temperature dependence of thermal conductivity.[16] The Seebeck coefficients are 124 and 150 μV K^{-1} for the p-type and n-type samples at 175 and 250 °C, respectively (Figure 2D).

The overall power generated from the TEG largely depends on the efficiency of the materials as well as the heat transfer. The efficiency of the material is estimated from the figure-of-merit inherent: $ZT = \sigma S^2 T/\kappa$, which depends on the electrical conductivity σ, Seebeck coefficient S, temperature T, and thermal conductivity κ. The ZT values are 0.29 and 0.10 for p-type and n-type at RT, respectively, and reach 0.53 for p-type at 175 °C and 0.55 for n-type at 250 °C (Figure 2E). The scanning electron micrograph (SEM) image in Figure 2F shows the nanolayered structure of Sb_2Te_3 after hot pressing at 285 °C using 40 kN for 2 h. Hot pressing of n-type Bi_2Te_3 (2 h at 325 °C, 40 kN) also generated a layer nanostructure (Figure S4). The measurement direction is the same as the heat flow direction that is vertical with the crystal orientation. The hot-pressed cuboids with a layered structure show an enhanced ZT value by strong phonon scattering (Figure S4).[2,34] The internal resistance of S-TEG is related to the electrical resistance of p-n couples and the contact resistance (R_c) by the equation: $r = n \times \left(\frac{1}{\sigma_p} \times \frac{l_p}{A_p} \times \frac{1}{\sigma_n} \times \frac{l_p}{A_p}\right) + R_c$where A is the cross-sectional area and l is length of TE cuboids, n is the number of p-n couples, and σ is the electrical conductivity.[35] Key features to control the internal resistance are the welding of the stretchable electrodes and TE cuboids together with the solder paste. The resistance of each p-n couple is 0.14 Ω, which includes 0.1 Ω for *p*-type legs and 0.04 Ω for *n*-type legs. The total resistance of the S-TEG with 50 pairs of TE elements is 22 Ω. Accordingly, the contact resistance is 21.8 Ω for 50 pairs (4.83 Ω for 18 pairs and 2.06 Ω for 9 pairs, respectively). Note that the ZT value of our S-TEG is comparable with the traditional TEG while the internal resistance is lower than the other types of semiflexible TEG like shape-conformal or organic TEG.[24,25,27,28]

To explore the device performance under different deformation states, we first studied the stability of internal resistance under stretching along the X and Y directions. The mechanical properties of the device can be visualized by deforming a 2 × 2 array unit (see Methods). The serpentine geometrical designs of electrodes minimize strain in the active materials. The horseshoe serpentines show an in-plane unraveling and out-of-plane buckling process during the stretching process, while the strain in the active component is limited.[36] The optical images show the excellent stretchability of the S-TEG in the X and Y directions (Figure 3A, 3B). The finite element analysis (FEA) shows that the biaxial strains correspond well with the experimental results. The maximum local strain is ~3.8% for the Cu electrodes. For

https://dx.doi.org/10.1021/acs.nanolett.0c01225
Nano Lett. 2020, 20, 4445−4453

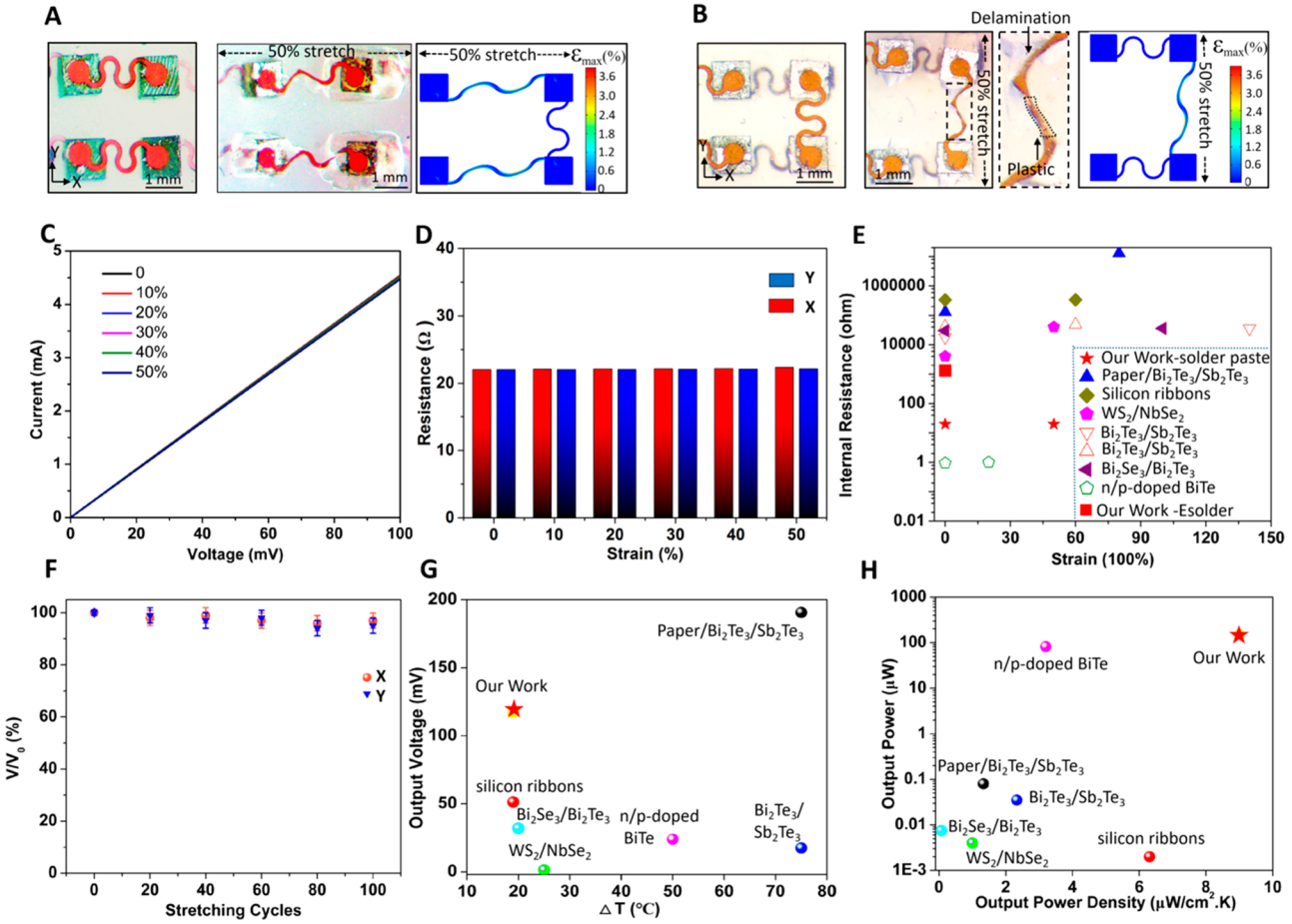

Figure 3. Electromechanical characterization of S-TEG. (A, B) Optical images and finite element analysis (FEA) of S-TEG under 50% biaxial tensile strains in the two different directions (*X* and *Y*). The color scale illustrates the local strain level in the device; (C) *I*−*V* curves of the S-TEG with different strains in the *X* directions. (D) Resistance changes of the stretchable TEG with different strain in two directions (*X* and *Y*); (E) Comparison of the internal resistance of S-TEG by using solder paste with other stretchable TEGs; a similar device made with esolder was made for comparison. (F) Normalized output voltage of S-TEG under stretching (50% strain) for over 100 cycles in two directions. Comparisons of the output voltage (G) and the output power vs output power density (H) of our S-TEG with other stretchable TEGs (see Table S1, all of the data from our work and the references were calculated based on the area of the thermoelectric components for comparison).

the serpentine electrodes, the irreversible deformation and the local delamination between the interconnects and silicone elastomers occurred when S-TEG was stretched over the yield point, which may decay the device robustness by generating some cracks.[37] Below 40% biaxial stretching, the S-TEG keeps good mechanical integrity (Figures S6, S7, and S8).[38] The serpentines broke with 80% strain, but the welding of the electrodes and the TE cuboids using solder paste did not break, demonstrating the strong bonding between them (Figure S9). The waterproof encapsulating films ensured the long-term reliability of the device for wearable and engineering applications (Figure S10).

For the wearable applications, the stretchable TEG should be mechanically endurable above 30% strain to accommodate a diverse of dynamic motions (bending, stretching, and twisting) of the human skin.[39] The *I*−*V* curves of the S-TEG keep almost the same up to 50% strain in the *X*-direction (Figure 3C). The result shows <1% change in the internal resistance and output voltage within the maximum strain in both directions (Figure 3D and Figure S11). As a comparison, we used Esolder 3022 to assemble the same amount of TE cuboids, and the internal resistance is ∼1K ohm, which is much higher than that of S-TEG using solder paste (Figure 3E). The smaller resistance using solder paste is attributed to an alloy formed between the solder paste and electrodes of thermoelectric cuboids. Repetitions of the stretch loadings also show that the device exhibits stable internal resistance and output voltage over 100 times with a 40% strain in the biaxial directions (Figure 3F and Figure S11). The results demonstrate the reliability of our S-TEG under stretch and can properly work on curved and dynamic heat sources. A comparison of our S-TEG with previously developed stretchable TEGs shows improvements on the output voltage and power, demonstrating improved performance of our S-TEG (Figure 3G, 3H and Table S1).

Hot sources with irregular curved surfaces are ubiquitous in real-world cases. To test the performance of the S-TEG on the developable surface, the S-TEG was attached to the polyvinyl chloride (PVC) pipes with different radii (Figure 4A). An open-circuit voltage of V_{oc} = 123.3 mV and power of 173 μW from the S-TEG (10 × 10 array) on tube 1 (radius R_1 = 14 mm) were obtained at a temperature difference of ΔT = 18.5 K (Figure 4B). For tube 2 with a larger radius (R_2 = 17 mm), an open-circuit voltage of V_{oc} = 122.1 mV and a power of 169.2 μW were obtained at ΔT = 19.8 K (Figure S12). The power density P_{max}/S is ∼0.17 mW/cm^2 at ΔT ∼ 19 K (*S* is the total

https://dx.doi.org/10.1021/acs.nanolett.0c01225
Nano Lett. 2020, 20, 4445−4453

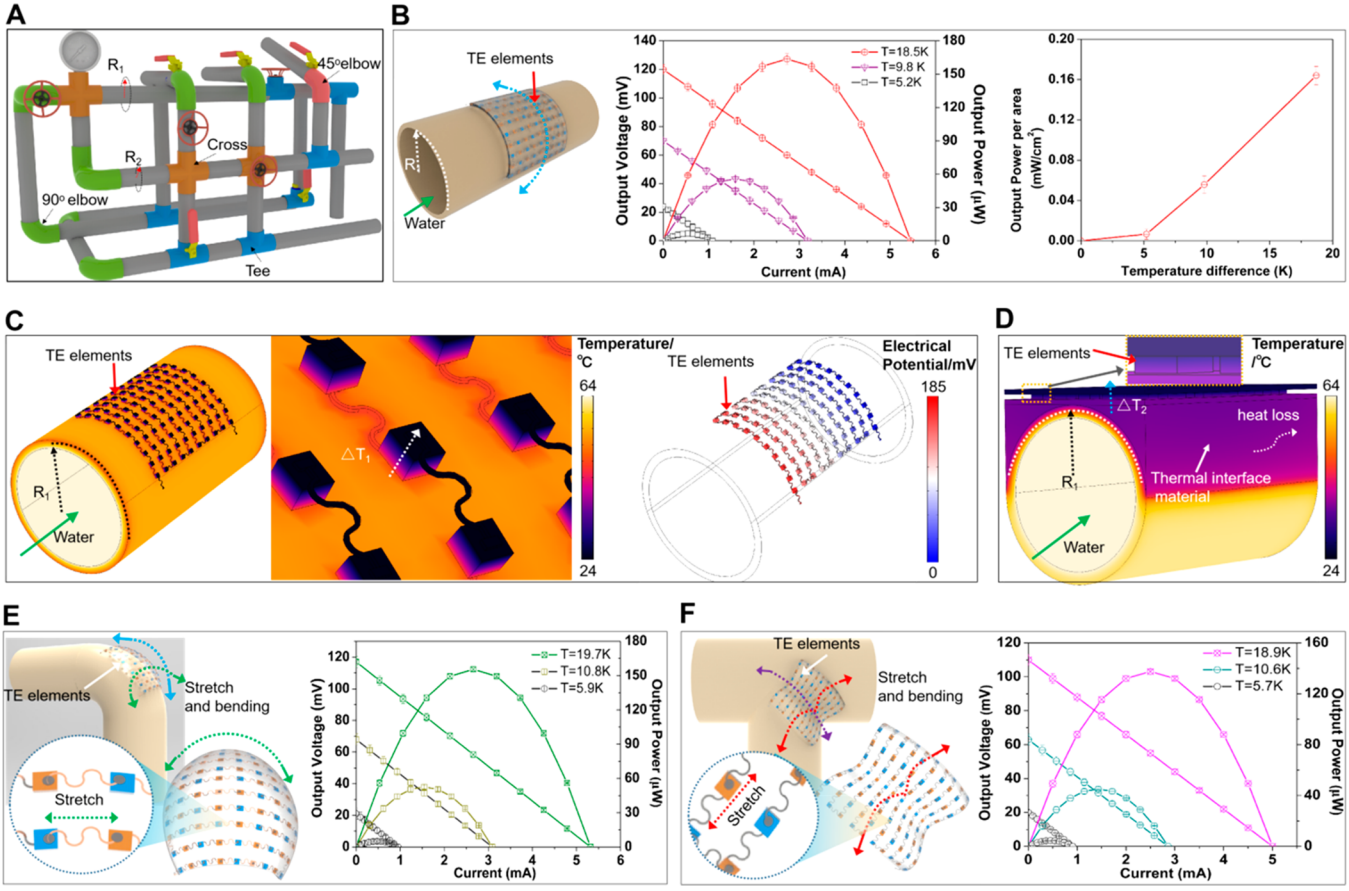

Figure 4. S-TEG integrated with complex static surfaces. (A) Schematic diagram shows hot water pipes with 45° and 90° elbows, tee, and cross joints. (B) Seebeck voltage generated on the tubes with a diameter of R_1 = 28 mm and output voltage and power of S-TEG at various temperature differences on tube 1. Schematic diagrams show the heat transfer and output voltage of the S-TEG (C) and the conventional planar TEG (D) on a developable surface that were simulated using Comsol Multiphysics, showing the larger heat storage and energy conversion of S-TEG. (E) S-TEG attached on a 90-degree elbow and the output voltage and power with temperature differences. (F) S-TEG attached on a tee joint and the output voltage and power with temperature differences, showing the excellent thermoelectric performance of S-TEG on a nondevelopable surface.

cross-sectional area of the TE elements). The results demonstrate the good conformability of S-TEG on heat sources with different curvatures. Comsol Multiphysics was used to simulate the heat transfer between the curved heat source and the two different types of TEGs, i.e., the S-TEG and the planar TEG with additional thermal interface material. The simulation shows ~1.6 times higher temperature difference for the S-TEG (ΔT_1) compared with the planar TEG (ΔT_2) on the developable surface (Figure 4C, 4D and Figure S13). The external supporting substrate for the planar TEG to attach to the curved surface caused heat loss and therefore degradation of the energy conversion (Figure 4D). The theoretical output voltage is determined by $V_{TH} = n \times (S_n + S_p) \times \Delta T$, where n is the number of the p-n junctions, and S_p and S_n are absolute Seebeck coefficients of p- and n-type cuboids, respectively.[35,40] The maximum output power from the S-TEG is $P_0 = (n(S_n + S_p) \times \Delta T)^2/(4R_{TEG})$, where R_{TEG} represents the internal resistance.[26] The comparison of the output voltage and power between experimental, theoretical, and calibrated results is discussed in Figure S14.

Most flexible TEGs can only work on developable surfaces but are hard to attach well on nondevelopable surfaces, especially for the elbows and joints that require the device to be stretched 30~40%.[38] To further demonstrate the application of the S-TEG on nondevelopable surfaces, we attached the device on a 90-degree elbow and a tee joint. The results show excellent attachment and performance of S-TEG on these nondevelopable surfaces that are challenging for traditional planar and flexible TEGs (Figure S15). The open-circuit voltage and output power per area for S-TEG on the elbow increases with the increment of ΔT, reaching 117 mV and 0.15 mW/cm^2, respectively, at ΔT = 19.7 K (Figure 4E). The open-circuit voltage and power of S-TEG on the tee joint are 110 mV and 137.5 μW (ΔT = 18.9 K), respectively (Figure 4F). The excellent performance of S-TEG on both the developable and nondevelopable hot surfaces is attributed to its outstanding stretchability to guarantee the surface attachment and the heat transfer from the waste heat that is critical for energy harvesting.

The S-TEG performed well on human skin that was not only complex and highly curved but also time dynamic. Wearable devices pose an important application for TEG since the human skin and the ambient temperature provide a natural temperature difference from which energy can be harvested (Figure 5A). During the movement of fingers and wrist, the output voltages show slight changes (<3%), demonstrating good attachment of the S-TEG on these dynamic surfaces (Figure 5B). Temperature changes of the bottom surfaces of the S-TEG and the planar TEG attached on a bending finger

https://dx.doi.org/10.1021/acs.nanolett.0c01225
Nano Lett. 2020, 20, 4445−4453

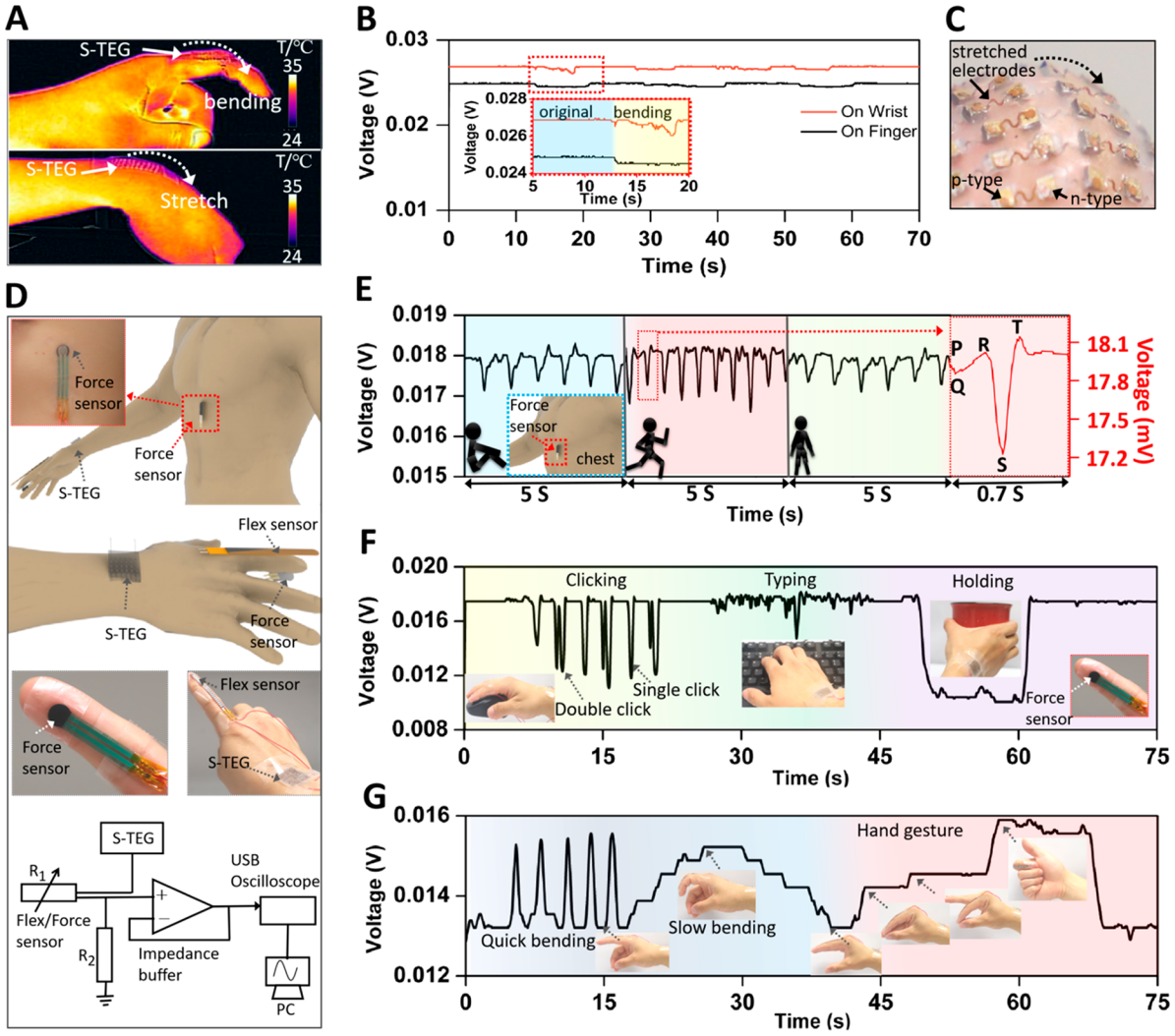

Figure 5. Performance of S-TEG with dynamic hot surfaces. (A) Infrared images of S-TEG on the human finger and wrist to demonstrate the device on dynamic hot surfaces. (B) Energy harvesting of S-TEG on dynamic surfaces of the human body. (C) Enlarged picture shows the attachment of S-TEG on a bending finger with stretched electrodes and silicon capsules. (D) Demonstrations and the related electronic circuit design of S-TEG as the energy solution for wearable devices. (E) Snapshots of a force sensor (force sensitive resistor) attached on the chest connected with the S-TEG (attached on wrist) to detect the heart rate for health monitoring at different times (red dash line shows the enlarged plot of a time period during running). The tests for resting, walking, and running were conducted separately, and the snapshots were assembled together in the figure. (F) A force sensor connected with the S-TEG (attached on the wrist) to detect the pressure of the finger during working and drinking (with R_2 equals to 50 KΩ). (G) A flex sensor (bending sensitive resistor) connected with the S-TEG (attached on the wrist) to detect the motion of the finger and different hand gestures (with R_2 equals to 10 KΩ).

were monitored using a cool airflow on the top surfaces of both TEGs. The results show that the temperature keeps almost constant ($\Delta T \sim 5.5$ °C) for the S-TEG while decreasing for the planar-TEG during movement (Figure S16). The electrodes and silicon matrix are both stretched, which enable the S-TEG modules to firmly adhere to the curved surface of the finger and guarantee efficient heat transfer during the finger movement (Figure 5C). In comparison, the existing planar or flexible TEGs cannot continuously contact the finger during movements, which causes large heat loss and significant reduction of the power generation efficiency.[41−43]

The S-TEG was also tested as an energy solution for wearable devices. Figure 5D shows the schematic diagram and the electronic circuit design to connect S-TEG with the flex (a bending sensitive resistor) and force sensor (a force sensitive resistor) in series. The initial resistance of the force sensor was R_1 = 1 MΩ, and the resistance will decrease with the increasing pressure. With a constant value of R_2 = 50 KΩ, the output voltage changed with the pressure. The S-TEG was used to harvest energy from the dynamic human wrist. It provided a voltage signal for the force sensor attached on the chest to monitor the heart rate with the output voltage of ∼27 mV (Figure 5B). The results show successful detection of different heart rates when at rest (75 bpm), running (120 bpm), and walking (78 bpm) with clearly identifiable sequences of Q, R, and S waveforms, which demonstrates the capability of S-TEG for health monitoring (Figure 5E).[44] The S-TEG can also be used to provide a voltage signal for the force sensor to detect the pressure on the finger when clicking the mouse (double click and single click), typing, holding water cup (Figure 5F), detecting the quick bending and slow bending of the finger, and even hand gestures (Figure 5G). The results indicate that body heat harvested by the S-TEG on the dynamic surface offers a potential energy solution to provide a voltage signal for

https://dx.doi.org/10.1021/acs.nanolett.0c01225
Nano Lett. 2020, 20, 4445−4453

the wearable devices for health monitoring, pressure detection, and gesture recognition. The stretchable property of S-TEG shows potential applications where the heat source might be in constant movement.[21,31] The S-TEG could also accommodate the complex motions of the human body via the integration with smart clothing, fabrics, and wearable self-powering devices in the future.[21,45−48]

In summary, we have presented the design and fabrication of a stretchable TEG that can conform to complex and dynamic heat source surfaces. Hot-pressing of TE powders leads to the high performance of p-n elements, and the wavy serpentine conductive network endows large stretchability to the device. The compliant substrate and electrodes guarantee good attachment of the S-TEG on complex curvilinear hot surfaces during movement. This S-TEG shows excellent performance on both developable and nondevelopable surfaces. Its performance is markedly superior to those of the previously reported S-TEGs. The energy harvesting of S-TEG from the dynamic surfaces of the human body offers a potential energy solution for wearable health-care electronics. The S-TEG device could be easily scaled up by doubling p-n couples or in series by connecting multiple modules to fabricate large-scale TEG devices for the energy harvesting of waste heat from daily life and industrial engineering.

■ ASSOCIATED CONTENT

Supporting Information

The Supporting Information is available free of charge at has been provided in the Supporting Information (PDF). The Supporting Information is available free of charge at https://pubs.acs.org/doi/10.1021/acs.nanolett.0c01225.

Further information about methods of fabrication of TE cuboids, fabrication of the stretchable thermoelectric device, mechanical testing of the device, materials characterizations and TE properties, FEA analysis, and test of wearable sensor connected with S-TEG (PDF)

■ AUTHOR INFORMATION

Corresponding Authors

Yong Chen − *Epstein Department of Industrial and Systems Engineering, Viterbi School of Engineering and Department of Aerospace and Mechanical Engineering, Viterbi School of Engineering, University of Southern California, Los Angeles, California 90089, United States*; Email: yongchen@usc.edu

Sheng Xu − *Materials Science and Engineering Program, Department of Mechanical and Aerospace Engineering and Department of NanoEngineering, University of California San Diego, La Jolla, California 92093−0418, United States*; Email: shengxu@ucsd.edu

Ziyu Wang − *The Institute of Technological Sciences, Wuhan University, Wuhan 430072, China*; orcid.org/0000-0001-9718-1263; Email: zywang@whu.edu.cn

Authors

Yang Yang − *Department of Mechanical Engineering, San Diego State University, San Diego, California 92182, United States*; orcid.org/0000-0002-4032-5446

Hongjie Hu − *Materials Science and Engineering Program, Department of Mechanical and Aerospace Engineering, University of California San Diego, La Jolla, California 92093−0418, United States*

Zeyu Chen − *State Key Laboratory of High Performance Complex Manufacturing, College of Mechanical and Electrical Engineering, Central South University, Hunan 410083, China*

Laiming Jiang − *Roski Eye Institute Keck School of Medicine, University of Southern California, Los Angeles, California 90033, United States*

Gengxi Lu − *Department of Biomedical Engineering, Viterbi School of Engineering, University of Southern California, Los Angeles, California 90089, United States*

Xiangjia Li − *Department of Aerospace and Mechanical Engineering, School for Engineering of Matter, Transport and Energy, Arizona State University, Tempe, Arizona 85281, United States*

Ruimin Chen − *Department of Biomedical Engineering, Viterbi School of Engineering, University of Southern California, Los Angeles, California 90089, United States*

Jie Jin − *Epstein Department of Industrial and Systems Engineering, Viterbi School of Engineering, University of Southern California, Los Angeles, California 90089, United States*

Haochen Kang − *Department of Biomedical Engineering, Viterbi School of Engineering, University of Southern California, Los Angeles, California 90089, United States*

Hengxi Chen − *Department of Chemical Engineering and Materials Science, University of Southern California, Los Angeles, California 90089, United States*

Shuang Lin − *Department of Chemical Engineering and Materials Science, University of Southern California, Los Angeles, California 90089, United States*

Siqi Xiao − *Department of Chemical Engineering and Materials Science, University of Southern California, Los Angeles, California 90089, United States*

Hanyu Zhao − *Department of Aerospace and Mechanical Engineering, Viterbi School of Engineering, University of Southern California, Los Angeles, California 90089, United States*

Rui Xiong − *School of Physics and Technology, Wuhan University, Wuhan 430072, China*

Jing Shi − *School of Physics and Technology, Wuhan University, Wuhan 430072, China*

Qifa Zhou − *Department of Biomedical Engineering, Viterbi School of Engineering, University of Southern California, Los Angeles, California 90089, United States*

Complete contact information is available at: https://pubs.acs.org/10.1021/acs.nanolett.0c01225

Author Contributions

[@]These authors contributed equally to this work.

Author Contributions

Y.Y., H.H., and Z.C. conceived and designed experiments. Y.Y., Z.C., H.H., and L.J. performed experiments, data collection, and analysis. R.C., H.C., and S.L. did the hot pressing and dicing. X.L., G.L., and H.Z. performed the mechanical and heat transfer simulation by Comsol Multiphysics. X.L. and Y.Y. performed the test of SEM images. Y.Y., J.J., and H.K. did the test of S-TEG for the energy solution for wearable device. Y.Y., Z.C., and H.H. wrote the manuscript. Y.C., S.X., Z.W., Q.Z., and Y.Y. planned, supervised, and led the project. All authors contributed to the discussion on the manuscript.

Notes

The authors declare no competing financial interest.

https://dx.doi.org/10.1021/acs.nanolett.0c01225
Nano Lett. 2020, 20, 4445−4453

■ ACKNOWLEDGMENTS

This work was supported by the National Science Foundation (NSF) (CMMI 1151191 and CMMI 1663663) and by USC's Epstein Institute and Honda Research Institute-USA.

■ REFERENCES

(1) Kim, S. I.; et al. Dense dislocation arrays embedded in grain boundaries for high-performance bulk thermoelectrics. *Science* **2015**, *348*, 109.
(2) Poudel, B.; et al. High-thermoelectric performance of nanostructured bismuth antimony telluride bulk alloys. *Science* **2008**, *320*, 634.
(3) Hightower, M.; Pierce, S. A. The energy challenge. *Nature* **2008**, *452*, 285.
(4) Chu, S.; Cui, Y.; Liu, N. The path towards sustainable energy. *Nat. Mater.* **2017**, *16*, 16.
(5) Tour, J. M.; Kittrell, C.; Colvin, V. L. Green carbon as a bridge to renewable energy. *Nat. Mater.* **2010**, *9*, 871.
(6) Vining, C. B. An inconvenient truth about thermoelectrics. *Nat. Mater.* **2009**, *8*, 83.
(7) Bell, L. E. Cooling, heating, generating power, and recovering waste heat with thermoelectric systems. *Science* **2008**, *321*, 1457.
(8) Straub, A. P.; Yip, N. Y.; Lin, S.; Lee, J.; Elimelech, M. Harvesting low-grade heat energy using thermo-osmotic vapour transport through nanoporous membranes. *Nature Energy* **2016**, *1*, 16090.
(9) Hochbaum, A. I.; et al. Enhanced thermoelectric performance of rough silicon nanowires. *Nature* **2008**, *451*, 163.
(10) Venkatasubramanian, R.; Siivola, E.; Colpitts, T.; O'quinn, B. Thin-film thermoelectric devices with high room-temperature figures of merit. *Nature* **2001**, *413*, 597.
(11) Kim, G.-H.; Shao, L.; Zhang, K.; Pipe, K. P. Engineered doping of organic semiconductors for enhanced thermoelectric efficiency. *Nat. Mater.* **2013**, *12*, 719.
(12) Chen, Y.; Zhao, Y.; Liang, Z. Solution processed organic thermoelectrics: towards flexible thermoelectric modules. *Energy Environ. Sci.* **2015**, *8*, 401.
(13) Zhang, Q.; Sun, Y.; Xu, W.; Zhu, D. Organic thermoelectric materials: emerging green energy materials converting heat to electricity directly and efficiently. *Adv. Mater.* **2014**, *26*, 6829.
(14) Suarez, F.; Nozariasbmarz, A.; Vashaee, D.; Öztürk, M. C. Designing thermoelectric generators for self-powered wearable electronics. *Energy Environ. Sci.* **2016**, *9*, 2099.
(15) Hong, S.; et al. Wearable thermoelectrics for personalized thermoregulation. *Science Advances* **2019**, *5*, No. eaaw0536.
(16) Snyder, G. J.; Toberer, E. S. Complex thermoelectric materials. *Nat. Mater.* **2008**, *7*, 105.
(17) Koumoto, K.; et al. Thermoelectric ceramics for energy harvesting. *J. Am. Ceram. Soc.* **2013**, *96*, 1.
(18) Ma, Y.; et al. Enhanced thermoelectric figure-of-merit in p-type nanostructured bismuth antimony tellurium alloys made from elemental chunks. *Nano Lett.* **2008**, *8*, 2580.
(19) Li, J.; et al. BiSbTe-based nanocomposites with high ZT: the effect of SiC nanodispersion on thermoelectric properties. *Adv. Funct. Mater.* **2013**, *23*, 4317.
(20) Deng, Y.; Liu, X.; Chen, S.; Tong, N. Thermal optimization of the heat exchanger in an automotive exhaust-based thermoelectric generator. *J. Electron. Mater.* **2013**, *42*, 1634.
(21) Rojas, J. P.; et al. Micro and nano-engineering enabled new generation of thermoelectric generator devices and applications. *ECS J. Solid State Sci. Technol.* **2017**, *6*, N3036.
(22) Wang, Y.; et al. *Adv. Mater.* **2019**, *31*, 1807916.
(23) Kim, F.; et al. 3D printing of shape-conformable thermoelectric materials using all-inorganic Bi 2 Te 3-based inks. *Nature Energy* **2018**, *3*, 301.
(24) Park, S. H.; Jo, S.; Kwon, B.; Kim, F.; Ban, H. W.; Lee, J. E.; Gu, D. H.; Lee, S. H.; Hwang, Y.; Kim, J.-S.; Hyun, D.-B.; Lee, S.; Choi, K. J.; Jo, W.; Son, J. S. High-performance shape-engineerable thermoelectric painting. *Nat. Commun.* **2016**, *7*, 13403.
(25) Kim, S. J.; We, J. H.; Cho, B. J. A wearable thermoelectric generator fabricated on a glass fabric. *Energy Environ. Sci.* **2014**, *7*, 1959.
(26) Jung, K. K.; Jung, Y.; Choi, C. J.; Lee, J. M.; Ko, J. S. Flexible thermoelectric generator with polydimethyl siloxane in thermoelectric material and substrate. *Curr. Appl. Phys.* **2016**, *16*, 1442.
(27) Park, T.; Park, C.; Kim, B.; Shin, H.; Kim, E. Flexible PEDOT electrodes with large thermoelectric power factors to generate electricity by the touch of fingertips. *Energy Environ. Sci.* **2013**, *6*, 788.
(28) Oh, J. Y.; et al. Chemically exfoliated transition metal dichalcogenide nanosheet-based wearable thermoelectric generators. *Energy Environ. Sci.* **2016**, *9*, 1696.
(29) Nan, K.; et al. Compliant and stretchable thermoelectric coils for energy harvesting in miniature flexible devices. *Science Advances* **2018**, *4*, No. eaau5849.
(30) Rojas, J. P.; et al. Paper based origami flexible and foldable thermoelectric nanogenerator. *Nano Energy* **2017**, *31*, 296.
(31) Rojas, J. P.; et al. Stretchable helical architecture inorganic-organic hetero thermoelectric generator. *Nano Energy* **2016**, *30*, 691.
(32) Xu, S.; et al. Assembly of micro/nanomaterials into complex, three-dimensional architectures by compressive buckling. *Science* **2015**, *347*, 154.
(33) Huang, Z.; et al. Three-dimensional integrated stretchable electronics. *Nature Electronics* **2018**, *1*, 473.
(34) Soni, A.; Yanyuan, Z.; Ligen, Y.; Aik, M. K. K.; Dresselhaus, M. S.; Xiong, Q. Enhanced Thermoelectric Properties of Solution Grown $Bi_2Te_{3-x}Se_x$ Nanoplatelet Composites. *Nano Lett.* **2012**, *12*, 1203.
(35) Chen, Y.; He, M.; Tang, J.; Bazan, G. C.; Liang, Z. Flexible Thermoelectric Generators with Ultrahigh Output Power Enabled by Magnetic Field–Aligned Metallic Nanowires. *Advanced Electronic Materials* **2018**, *4*, 1800200.
(36) Xu, S.; et al. Stretchable batteries with self-similar serpentine interconnects and integrated wireless recharging systems. *Nat. Commun.* **2013**, *4*, 1543.
(37) Zhang, Y.; et al. Experimental and theoretical studies of serpentine microstructures bonded to prestrained elastomers for stretchable electronics. *Adv. Funct. Mater.* **2014**, *24*, 2028.
(38) Hu, H.; et al. Stretchable ultrasonic transducer arrays for three-dimensional imaging on complex surfaces. *Science Advances* **2018**, *4*, No. eaar3979.
(39) Kim, D.-H.; Ghaffari, R.; Lu, N.; Rogers, J. A. Flexible and stretchable electronics for biointegrated devices. *Annu. Rev. Biomed. Eng.* **2012**, *14*, 113.
(40) Wu, G.; et al. Exploring high-performance n-type thermoelectric composites using amino-substituted rylene dimides and carbon nanotubes. *ACS Nano* **2017**, *11*, 5746.
(41) Kim, M.-K.; Kim, M.-S.; Lee, S.; Kim, C.; Kim, Y.-J. Wearable thermoelectric generator for harvesting human body heat energy. *Smart Mater. Struct.* **2014**, *23*, 105002.
(42) Francioso, L.; et al. PDMS/Kapton interface plasma treatment effects on the polymeric package for a wearable thermoelectric generator. *ACS Appl. Mater. Interfaces* **2013**, *5*, 6586.
(43) Yang, Y.; Lin, Z.-H.; Hou, T.; Zhang, F.; Wang, Z. L. Nanowire-composite based flexible thermoelectric nanogenerators and self-powered temperature sensors. *Nano Res.* **2012**, *5*, 888.
(44) Xu, S.; et al. Soft Microfluidic Assemblies of Sensors, Circuits, and Radios for the Skin. *Science* **2014**, *344*, 70.
(45) Park, H.; et al. Mat-like flexible thermoelectric system based on rigid inorganic bulk materials. *J. Phys. D: Appl. Phys.* **2017**, *50*, 494006.
(46) Khan, Y.; Ostfeld, A. E.; Lochner, C. M.; Pierre, A.; Arias, A. C. Monitoring of vital signs with flexible and wearable medical devices. *Adv. Mater.* **2016**, *28*, 4373.
(47) Zheng, W.; et al. Low thermal conductivity and high thermoelectric figure of merit in p-type Sb_2Te_3/poly(3,4-ethylenedioxythiophene) thermoelectric composites. *Appl. Phys. Lett.* **2014**, *105* (2), 023901–023901–4.

https://dx.doi.org/10.1021/acs.nanolett.0c01225
Nano Lett. 2020, 20, 4445–4453

(48) huang, S.; Wang, Z.; Xiong, R.; Yu, H.; Shi, J. Significant enhancement in thermoelectric performance of Mg_3Sb_2 from bulk to two-dimensional mono layer. *Nano Energy* **2019**, *62*, 212.

https://dx.doi.org/10.1021/acs.nanolett.0c01225
Nano Lett. 2020, 20, 4445−4453